Effects of atmospheric dynamics and aerosols on the fraction of supercooled water clouds

Jiming Li[1], Qiaoyi Lv[1], Min Zhang[1], Tianhe Wang[1],
Kazuaki Kawamoto[2] and Siyu Chen[1]

[1]Key Laboratory for Semi-Arid Climate Change of the Ministry of Education, College of Atmospheric Sciences, Lanzhou University, Lanzhou, China

[2]Graduate School of Fisheries Science and Environmental Studies, Nagasaki University, Nagasaki, Japan

Running Head: Effects of dynamics and aerosols on the cold cloud phase

Corresponding author: Jiming Li, Key Laboratory for Semi-Arid Climate Change of the Ministry of Education, College of Atmospheric Sciences, Lanzhou University, Lanzhou, Gansu 730000, China. (lijiming@lzu.edu.cn)

Abstract

Based on the 8 years (2007-2015) of data of cloud phase information from the GCM-Oriented Cloud-Aerosol Lidar and Infrared Pathfinder Satellite Observation (CALIPSO) Cloud Product (GOCCP), aerosol products from CALIPSO, and meteorological parameters from the ERA-Interim products, this study investigates the effects of atmospheric dynamics on the supercooled liquid cloud fraction (SCF) under different aerosol loadings at a global scale in order to better understand the conditions under which supercooled liquid water will gradually transform to ice phase.

Statistical results indicate that aerosols' effect on nucleation cannot fully explain all SCF changes, especially in those regions where aerosols' effect on nucleation is not a first-order influence (e.g., due to low IN aerosol frequency). By performing the temporal and spatial correlations between SCFs and different meteorological factors, we find that the impacts of different meteorological factors on SCFs contain obvious regional differences. In the tropics, obvious positive correlations between SCFs and vertical velocity and relative humidity indicate that high vertical velocity and relative humidity suppress ice formation. However, the impacts of LTSS, skin temperature and horizontal wind on SCFs are relatively complex than those of vertical velocity and humidity. But, their effects are predominantly located in middle and high latitudes, and the temporal correlations with SCFs depend on latitude or surface type. In addition, this study also indicates that strong horizontal wind inhibits the glaciation of supercooled droplets in the middle and high latitudes. Our results verify the importance and regional of dynamical factors on the changes of supercooled water cloud fraction, thus have potential implications for further improving the parameterization of the cloud phase and determining the climate feedbacks.

1. Introduction

Cloud radiative feedbacks are recognized as the greatest uncertainty in the climate change predictions made by climate models (Andrews et al., 2012). Cloud phase, an important cloud property, can directly affect the Earth's radiation budget and climate. For example, liquid water clouds exert a net cooling effect by significantly reflecting the incident shortwave radiation, whereas thin cirrus clouds tend to have a net warming effect as their greenhouse effect overcomes their albedo effect. In view of the entirely different radiative properties of ice and liquid particles, changes in the liquid-ice phase transition will significantly affect the Earth's radiation budget and precipitation efficiency (Fu et al., 1999; Fu, 2007; Sassen and Khvorostyanov, 2007; Forbes and Ahlgrimm, 2014; Sun et al., 2004, 2015). It is therefore of fundamental importance to know the spatiotemporal distributions of different cloud phases and examine their variation on a global scale for accurate calculations of cloud radiative effects.

Clouds are composed entirely of liquid or ice particles when temperatures are above the freezing (0 ℃) or below homogeneous freezing (approximately -40 ℃), respectively (Pruppacher and Klett, 1997). Between 0 ℃ and -40 ℃, clouds could be pure ice, liquid particles or a mixture. Liquid water clouds with temperatures lower than 0 ℃ are called supercooled water clouds. Previous studies have verified the existence of supercooled water at temperatures as low as -30 ℃ to -40 ℃ (e.g., Intrieri et al., 2002; Shupe et al., 2006; Morrison et al., 2011). For example, using un-polarized, ground-based Lidar data from Chilbolton in Southern England, Hogan et al. (2003) found that 27% of clouds between -5 ℃ and -10 ℃ in Chilbolton contain a supercooled liquid-water layer; this percentage falls steadily with temperature and reaches approximately zero at temperatures below -35 ℃. Giraud et al. (2001) used the Along-Track Scanning Radiometer (ATSR)-2 infrared data from the ERS-2 satellite to analyze the relationship between cloud phase and cloud top temperature. Their results indicated that the probability of ice phase clouds decreases quasi-linearly with cloud top temperature from nearly 100% at approximately -33 ℃ to close to 0% at -10 ℃.

The classic Wegener-Bergeron-Findeisen process suggested that ice crystals and liquid drops cannot coexist in equilibrium at sub-zero temperatures because the vapor pressure at the ice surface is smaller than that over liquid drops (Wegener, 1911; Bergeron, 1935; Findeisen, 1938). However, observations have verified that supercooled drops may coexist with ice crystals in mixed-phase clouds at temperatures as low as -40 ℃ (Borovikov et al., 963; Sassen 1992) typically for a few hours (Korolev et al., 2003) or even longer times (Boer et al., 2009). This result indicates that the ice growth rate (acting as a liquid sink) must be balanced by an equally strong condensate supply rate (liquid source) and that a continuous supply of new or recycled ice nuclei must be available (Forbes and Ahlgrimm, 2014). By assessing the radiative transfer impacts of mixed-phase clouds, Sassen and Khvorostyanov (2007) showed that the total cloud radiative impact of mixed-phase clouds decreases as supercooled clouds glaciate. Changing the phase description in a general circulation models (GCMs) could lead to biases not only on the radiative flux (Yun and Penner, 2012) but also in the zonal cloud fraction, the heating rate, the humidity, and the cloud water content (Cheng et al., 2012). A recent GCM intercomparison study indicated that the difference in albedo feedback among different models is primarily a result of the differences in the poleward redistribution of cloud liquid water due to differences in mixed-phase cloud algorithms (Tsushima at al., 2006): the models that produce more supercooled water clouds have a higher sensitivity. Thus, global statistics of the variations of supercooled liquid clouds caused by enhanced ice nuclei (Choi et al., 2010; Tan et al., 2014; Zhang et al., 2015) or changed environmental conditions (temperature, water vapor, vertical motion) will be helpful in improving the simulation of mixed-phase clouds in the current climate models and reduce uncertainties in cloud feedback within GCMs.

Compared with the passive remote sensing (Huang et al., 2005; 2006a), the millimeter-wavelength cloud-profiling radar (CPR) on CloudSat (Stephens et al., 2002) and the cloud-aerosol Lidar with orthogonal polarization (CALIOP) (Winker et al., 2007) on CALIPSO (launched in late April, 2006) can provide more accurate data regarding the vertical structure of clouds, along with cloud phase information on a

global scale (Hu et al., 2010; Li et al., 2010, 2015; Lv et al., 2015). The depolarization ratio and layer-integrated backscatter intensity measurements from CALIOP can help distinguish cloud phases (Hu et al., 2007, 2009). Using combined CALIOP/IIR/MODIS measurements, Hu et al. (2010) compiled global statistics regarding the occurrence, liquid water content and fraction of supercooled liquid clouds. Based on the vertically resolved observations of clouds and aerosols from CALIOP, Choi et al. (2010) and Tan et al. (2014) analyzed the variation of supercooled water cloud fraction and possible dust aerosol impacts at given temperatures. For dynamic processes, although some studies have focused on the impacts of meteorological parameters on supercooled water cloud fraction at regional or global scales (Naud et al., 2006; Cesana et al., 2015), systematic studies of the statistical relationship between cloud phase changes and meteorological parameters at a global scale have received far less attention. For the above reasons, this study combines cloud phase information from the GCM-Oriented Cloud-Aerosol Lidar and Infrared Pathfinder Satellite Observation (CALIPSO) Cloud Product (GOCCP) (Chepfer et al., 2010), meteorological parameters from ERA-interim reanalysis datasets and the aerosol product from CALIPSO to investigate the impacts of meteorological parameters on the supercooled liquid cloud fraction under different aerosol loadings at a global scale.

This paper is organized as follows: a brief introduction to all datasets used in this study is given in Section 2. Section 3.1 outlines the global distributions and seasonal variations of SCFs and IN aerosol (here, dust, polluted dust and smoke). Further analyses regarding the temporal and spatial correlations between SCFs and meteorological parameters are provided in section 3.2 and 3.3. Important conclusions and discussions are presented in Section 4.

2. Datasets and methods

In the current study, 8 years (2008–2015) of data from CALIPSO-GOCCP, the ERA-Interim daily product (Dee et al., 2011) and the CALIPSO level 2, 5 km aerosol layer product are collected to analyze the effects of meteorological parameters on the SCFs under different aerosol loadings at a global scale.

2.1 Cloud phase product

Currently, several methods have been presented to determine the thermodynamic phase at the cloud top based on Lidar-only or combined Radar-Lidar signals. For Radar-Lidar cloud phase products, DARDAR (Delanoe and Hogan, 2010; Ceccaldi et al., 2013) and CloudSat 2B-CLDCLASS-LIDAR (Zhang et al., 2010) cloud phase products take advantage of the combination of Lidar backscatter and radar reflectivity to distinguish ice clouds, typical mixed-phase clouds, where a liquid top overlies the ice, and liquid clouds. However, because non-spherical particles (ice crystal) can change the state of polarization of backscatter light, the standard CALIOP cloud phase product distinguishes the water and ice phases of a cloud by using the Lidar depolarization ratio and layer integrated attenuated backscattering coefficient (Hu et al., 2007, 2009). As another Lidar-only cloud climatology, the single goal of CALIPSO-GOCCP climatology is to facilitate the evaluation of clouds in climate models (e.g., Cesana and Chepfer, 2012; Cesana et al., 2015) with the joint use of the CALIPSO simulator (Chepfer et al., 2008). For this specific purpose, GOCCP has been designed to be fully consistent with the CALIPSO simulator included in the Cloud Feedback Model Intercomparison Project (CFMIP, http://www.cfmip.net) Observation Simulator Package (COSP) used within version 2 of the CFMIP (CFMIP-2) experiment (Bodas-Salcedo et al., 2011) and phase 5 of the Coupled Model Intercomparison Project (CMIP5, Taylor et al., 2012). In CALIPSO-GOCCP product, Cesana and Chepfer (2013) built a discrimination threshold to separate ice-dominated clouds and liquid-dominated clouds by using CALIPSO version 3 measurements of attenuated total backscatter and its cross-polarized component at a fixed vertical resolution of 480 m. Because Lidar cannot penetrate optically thick clouds (optical depth>3, such as the supercooled liquid layer in the polar region) to detect ice crystals (Zhang et al., 2010), the CALIPSO-GOCCP and standard CALIOP cloud phase products both possibly lead to a slight underestimation of ice clouds at the lowest levels at mid-latitudes and in polar regions (Cesana et al., 2015). Recently, Mlmenstadt et al. (2015) found that the global average disagreement between the DARDAR and CALIPSO-GOCCP cloud phase products is 5% for ice-topped and 1%

for liquid-topped clouds, with no strong regional variation.

In the current analysis, the cloud phase information is mainly derived from the 3D_CloudFraction_Phase_temp monthly average dataset in the CALIPSO-GOCCP cloud product. This dataset contains cloud fractions for all clouds and for liquid/ice clouds as a function of the temperature in each longitude/latitude grid box (2°×2°). The temperature is taken from GMAO data (Global Modeling and Assimilation Office, Bey et al., 2001), which is part of the CALIPSO level 1 ancillary data. For each CALIOP level 1 profile, the GMAO temperature is interpolated over the 480 m-vertical levels of CALIPSO-GOCCP as the cloudy pixel temperature. That is, the temperature bins are ranged every 3 ℃ and 38 temperature bins are provided for each parameter. Those liquid phase clouds whose high bounds of their temperature bins are lower than 0 ℃ are considered as supercooled water phase clouds. Here, we define the supercooled water cloud fraction (SCF) in a given temperature bin (or isotherm) as the ratio of the liquid cloud fraction and the total cloud fraction (liquid+ice) in a 2°×2° grid box. Because temperature has dominant influence on SCFs, the present study is performed for three fixed temperature bins, which represent -10 ℃, -20 ℃ and -30 ℃ isotherms.

2.2 Meteorological reanalysis dataset

The ERA-Interim reanalysis daily 6-hour product, obtained by spatial and temporal matching with the CALIPSO aerosol product, is used to provide the related information of meteorological parameters at the surface and several pressure levels. At the surface level, skin temperature, surface pressure and 2-m air temperature are extracted. In the pressure level product, vertical velocity at 500 hPa, relative humidity at three levels (400, 500 and 600 hPa), the u component of wind at 100 hPa and 700-hPa temperature are used in the current analysis. Here, the information of the 700 hPa temperature, surface pressure and 2-m air temperature are used to calculate the lower-tropospheric static stability (LTSS), which is defined as the difference in potential temperature between 700 hPa and the surface (Klein and Hartmann, 1993),

or $\Delta\theta = T_{700}\left(\frac{1000}{p_{700}}\right)^{R/C_p} - T_{sfc}\left(\frac{1000}{p_{sfc}}\right)^{R/C_p}$, where p is pressure, T is temperature, R is the gas constant of air, and C_p is the specific heat capacity at a constant pressure. A high LTSS value represents a stable atmosphere, whereas a low LTSS value represents an unstable atmosphere. These meteorological parameters are further processed as monthly grid data to perform the temporal and spatial correlations between them and SCFs in section 3.2 and 3.3.

2.3 Aerosol types and relative frequency

Aerosol data are obtained from the CALIPSO level 2, 5 km aerosol layer product. Using scene classification algorithms (SCAs), CALIPSO first classifies the atmospheric feature layer as either a cloud or aerosol by using the mean attenuated backscatter coefficients at 532/1064 nm, along with the color ratio (Liu et al., 2009). A confidence level for each feature layer is also reported for the level 2 products. Using the surface type, Lidar depolarization ratio, integrated attenuated backscattering coefficient and layer elevation, aerosols are further distinguished as desert dust, smoke, polluted dust, clean continental aerosol, polluted continental aerosol, and marine aerosol (Omar et al., 2009). Mielonen et al. (2009) used a series of Sun Photometers from the Aerosol Robotic Network (AERONET) to compare CALIOP and AERONET aerosol types and found that 70% of the aerosol types from these two datasets are similar, with the closest similarities occurring between dust and polluted dust types. Mineral dust from arid regions has been widely recognized as an important source of ice nuclei in mixed-phase clouds because of its nucleation efficiency and abundance in the atmosphere (Richardson et al., 2007; DeMott et al., 2010; Atkinson et al., 2013). In addition to dust, some studies have also verified the potential ice nucleation ability of polluted dust and smoke at cold temperatures (Niedermeier et al., 2011; Cziczo et al., 2013; Zhang et al., 2015). For example, by using satellite Lidar observations, Tan et al. (2014) found negative temporal and spatial correlations between the supercooled liquid cloud fraction and the polluted dust and smoke aerosol frequencies at the −10ºC, −15ºC, −20ºC, and −25ºC isotherms, although those correlations are weaker than those found between dust frequencies and the

supercooled liquid cloud fraction. However, because the main goal of this study is to discuss the impact of meteorological parameters on supercooled liquid clouds rather than the effectiveness of different aerosol types acting as ice nuclei, we thus combine the dust, polluted dust and smoke information from CALIPSO to calculate the total relative occurrence frequency (RAF) of these IN aerosol types. Given the difficulty of quantifying the concentration of IN aerosols, the relative occurrence frequency can be used as a proxy of the concentration of aerosols (Choi et al., 2010). In addition, we remove those aerosol layers with low confidence values (feature type QA flag as "low" in aerosol product) from the dataset (approximately 6.5% of all aerosol layers). To maintain consistent temperature bins in the CALIPSO-GOCCP cloud product, the aerosol layer top temperature is also taken from the GMAO data, which is part of the CALIPSO Level 2 ancillary data. Moreover, the partition and numbers of temperature bins (3℃ intervals) for the aerosol layer-top are also the same as those of the CALIPSO-GOCCP cloud product. For every IN aerosol sample, we first arrange a temperature bin for it based on its layer-top temperature. Then, following Choi et al. (2010), we define the frequency of IN aerosols at a given temperature bin as the ratio of the number of IN aerosol samples to the total number of observation profiles for the same temperature bin and grid. Finally, the relative occurrence frequencies of IN aerosols are calculated by normalizing aerosol frequencies. That is, aerosol frequencies are divided by the highest aerosol frequency at a given isotherm (temperature bin). The RAF of an aerosol is thus indicative of the temporal and spatial variability of IN aerosols compared to the maximum occurrence frequency (Choi et al., 2010).

Note that the global distributions and seasonal variations of SCFs and the RAFs in section 3.1 are the 8-year average values; thus, grid sizes of all parameters are set as 2 °latitude by 2 °longitude. However, to analyze the temporal and spatial correlation between SCFs and meteorological parameters under different aerosol loadings in section 3.2, we have to reduce the grid size to 10 °latitude by 10 °grid boxes to avoid the issue of a sparse dataset caused by the narrow orbit of CALIOP and provide enough long time series to calculate the temporal correlation between parameters.

Moreover, to avoid artifacts due to noise from scattering of sunlight, it is better to conduct the CALIOP retrieval during nighttime. However, in view of the lack of CALIPSO observations at high latitudes of the northern Hemisphere during boreal summer nights, this study utilizes the mean values of SCFs, meteorological parameters and RAFs during daytime and nighttime to perform the temporal and spatial correlations analysis.

3 Results

3.1 Global and seasonal distributions of 8-year average SCFs and RAFs

Based on the statistical results of the 8-year CALIPSO-GOCCP cloud phase product and CALIPSO level 2, 5 km aerosol layer product, the global distributions and seasonal variations of SCFs and the total relative occurrence frequencies of dust, polluted dust and smoke aerosols at three isotherms, i.e., −10ºC, −20ºC, and −30ºC, at a 2° latitude by 2° longitude resolution are provided in Fig. 1, Fig. 2 and Fig. 3, respectively. Here, the four boreal seasons are spring (March, April and May), summer (June, July and August), autumn (September, October and November) and winter (December, January and February), respectively. At the -10 ℃ isotherm (Fig. 1), supercooled water cloud fractions at middle and high latitudes of two hemispheres have large values. The SCFs can exceed 70% over the high latitudes (poleward of 60 °) during all seasons, except in Greenland. The SCFs at those regions between 30 °N and 30 °S range from 15% to approximately 50%; the lowest SCFs (<30%) are predominantly located in typical subsidence regions (e.g., stratocumulus regions), where weak subsidence favors low cloud formation and suppresses ice or mixed-phase cloud generation (Wood et al., 2012; Yuan and Oreopoulos, 2013). Moreover, low SCFs also occur in the northwest part of China during boreal spring and winter. For relative aerosol frequency at the -10 ℃ isotherm, global distributions are expected and a large RAF is predominantly located in the dust source regions, i.e., Saharan and Taklimakan Deserts, where dust relative frequencies are greater than 20% during boreal summer and spring, respectively. The "aerosol belt" near America (between 30 °N and 60 °N) during boreal spring is mostly from the long-range transport of dust from the Taklimakan Desert, which travels across the Pacific Ocean

to America via westerlies (Huang et al., 2008). Moreover, Saharan dust can also be transported by trade winds across the Atlantic to America and the Caribbean. At the −20 ℃ and -30 ℃ isotherms, the spatial distributions of SCFs are similar to those results at -10 ºC, and SCFs are lower at −20ºC and -30ºC than at −10ºC. However, the seasonal variation of SCFs at −20ºC and -30 ℃ are more obvious compared with those results at −10ºC, especially at high latitudes of the northern hemisphere. For RAFs, however, note that comparison between different isotherms is not meaningful because the RAFs are normalized relative to each fixed isotherm. Thus, larger RAF at -20 ℃ or 30 ℃ than at -10 ℃ does not mean that the true aerosol frequency at -20 ℃ or -30 ℃ is really higher than values at -10 ℃. Compared with the RAFs at the -10 ℃ isotherms, the "aerosol belt" between 30° and 60° for two hemispheres at the -20 ℃ or -30 ℃ isotherms is more apparent. Previous studies have verified that the regional differences in the SCFs at -20 ℃ or other isotherms are highly correlated with the dust frequency above the freezing level (Choi et al., 2010; Tan et al., 2014). However, based on Figs. 1-3, we find that this is not always the case for all regions. For example, the SCFs in the tropics maintain persistently low values at three isotherms throughout the whole year, even though the aerosol loading is very low in this region. Moreover, by analyzing the zonal means of SCFs and RAFs (Fig. 4), we find that the SCF still has a low value at the mid-latitudes of the northern hemisphere during the summer season, even though the IN aerosol loading is significantly low at -20 ℃ in these regions. The obvious seasonal variations of SCFs over these regions seem not to be explicitly related to the seasonal variation of aerosol frequency. These results indicate that the aerosols' effect on nucleation cannot fully explain all changes of the supercooled liquid cloud fraction in our study, especially its regional and seasonal variations. In other words, there is no evidence to suggest that the aerosol effect is always dominant for each isotherm. Then, can these variations of SCF contribute to the meteorological effect? If yes, what is the role of meteorological parameters in determining cloud phase change, especially at those regions in which the aerosol effect on nucleation isn't a first-order influence due to low IN aerosol frequency? In the following section, temporal and spatial correlation analysis between SCFs and

meteorological parameters is conducted to help address these questions.

3.2 Temporal Correlations between SCFs and meteorological parameters

To further understand and quantify the statistical relationship between each meteorological parameter and SCF over the 8-year period (96 months), we calculate the monthly averages of SCF, meteorological parameters and RAF at different isotherms (or pressure levels) of each grid box and determine the temporal correlations between monthly averages of these variables. Similar to the study of Tan et al. (2014), we also reduce the grid size to 10 ºlatitude by 10 ºlongitude grid boxes to increase the sample number and avoid the issue of a sparse dataset caused by the narrow orbit of CALIOP. Moreover, only values of those regions with temporal correlations between SCFs and meteorological parameters at the 95% confidence level are displayed in the following global maps, and spatial correlation is determined.

Fig. 5 shows the global distributions of temporal correlations between SCFs at three isotherms (-10 ℃, -20 ℃ and -30 ℃) and skin temperature, i.e., LTSS. For skin temperature (left panel), temporal correlation coefficients have obvious regional differences. For example, at the -10 ℃ isotherm, negative temporal correlations are mainly located in Europe and ocean regions between 30 ° and 60 ° in two hemispheres, whereas the positive correlations can be found in the tropics, Mainland China, and Greenland. With decreasing temperature (e.g., at the -20 ℃ isotherm), the negative temporal correlation coefficients between SCFs and skin temperature more widely distribute at middle and high latitudes. It means that high skin temperature promotes the glaciation of supercooled droplets at middle and high latitudes and inhibits the glaciation in the tropics for the -20 ℃ isotherm. In the tropics, high skin temperature tends to trigger tropical deep convection easily. The vigorous updrafts in convective clouds do not leave enough time for supercooled droplets to transform into ice crystals, thus suppressing ice formation or pushing supercooled liquid water to a colder cloud top height (Bower et al., 1996). Indeed, the obvious positive temporal correlations in the tropics between SCFs and the vertical velocity at 500 hPa provide support for this inference (see Fig. 6). However, for land regions of poleward of 30 °, the opposite seasonal cycles between SCFs and skin temperature correspond to the positive

correlations between SCFs and LTSS, such as, Europe, Greenland and North America (right panel of the Fig.5). The opposite correlations are more obvious at -30 ℃ isotherm. By analyzing the temporal correlations between SCFs at -30 ℃ isotherm and LTSS (right panel of Fig. 5) and the global distribution of LTSS and skin temperature (see Fig. s1 in the supplemental materials), we find that positive correlations usually exist for lands of middle or high latitudes except Greenland, where LTSS also maintains high values and obvious seasonal variations. However, although the seasonal cycles of LTSS are weak over ocean regions (Figure not shown), the negative correlations between SCFs and LTSS can still be observed over the ocean.

Following Fig. 5, Fig. 6 shows the temporal correlations between SCFs at three isotherms and 500-hPa vertical velocity and relative humidity at three pressure levels (400 hPa, 500 hPa and 600 hPa). Here, it worth noting that the positive vertical velocity in this study means updraft, whereas negative vertical velocity corresponds to downdraft. Cesana et al. (2015) found that rising air supports the ice crystals formation over liquid droplets for decreasing temperatures. The same trend is observed at different latitudes (tropics, midlatitudes, and poles). However, West et al. (2014) concluded that increasing the subgrid vertical velocity leads to an increase of the liquid water path. In this study, our results indicate that obvious positive correlations between SCFs and vertical velocity (or relative humidity) only locate in tropics. It means that large vertical velocity and relative humidity suppress ice formation. The relationship is particularly evident in the eastern Hemisphere (e.g., Africa), and the correlation coefficient may go beyond 0.7. Generally speaking, the impacts of vertical velocity and relative humidity on SCF variation gradually weaken (even vanish) as temperature decreases. Moreover, the impact of relative humidity on the variation of SCFs is more extensive and apparent than that of vertical velocity. Based on the low relative occurrence frequency and weak seasonal cycle of IN aerosols between -40 ℃ and 0 ℃ isotherms in the tropics, our results indicate that seasonal variations of SCFs at a given isotherm can be attributed to the effect of meteorological parameters, especially the vertical velocity and relative humidity.

Beyond the tropical region, the obvious impact of vertical velocity on cloud phase disappears, whereas relative humidity still has an effect (e.g., America), although only a small correlation coefficient exists. In addition to skin temperature, LTSS, vertical velocity and humidity, we find that horizontal wind speed at 100 hPa can also affect the SCFs, especially at the middle and high latitudes (see Fig. 7). Overall, stronger winds are correlated with an increase in SCFs at different isotherms for middle and high latitudes, whereas negative correlations also exist in central Africa, the Tibetan Plateau or poleward regions of 60 °S. Similar to vertical velocity and relative humidity, the relationship also gradually weakens (even vanishes) with decreasing temperature. Noel et al. (2010) indicated that the frequency of oriented crystal drops severely in areas dominated by stronger horizontal wind speed at 100 hPa. This effect is especially noticeable at latitudes below 40 °. Our results further indicate that the impact of horizontal wind on the SCFs also exists. In summary, the above analysis shows that the impacts of different meteorological factors on the supercooled liquid cloud fraction exist with obvious regional difference.

Time series plots of SCFs, meteorological parameters and RAFs of IN aerosol of several selected regions are displayed in Fig. 8, Fig. 9 and Fig. 10, respectively. Note that each line in every subplot corresponds to a time series of different variables after 5 months of smoothing; however, the coefficients (at the 95% confidence level) in subplots represent the temporal correlation between the original SCFs series and meteorological parameters (or RAFs). We also provide the confidence value (i.e., p value) when the confidence level of the temporal correlation between variables is less than 95%. Moreover, three selected regions represent different aerosol loadings. For example, Fig. 8 shows the time series of variables studied at the -30 ℃ isotherm over the central China (100 °E-110 °E, 30 °N-40 °N), which is nearby the Taklimakan Desert. High frequencies of dust and polluted dust in this region peak in months coinciding with months when SCFs are at minimum; their correlation coefficient is approximately -0.63. Negative correlations also exist between SCF and LTSS (or horizontal wind at 100 hPa); their values are -0.28 and -0.53, respectively. The seasonal cycle of skin temperature over this region also maintains better consistency

with the seasonal variation of SCFs (corrcoef=0.5). At the -10 ℃ isotherm over a region near the Bahamas (70 ℃W-60 ℃W, 20 ℃N-10 ℃N), the RAFs of aerosol are persistently low (<0.02) for 96 months (see Fig.9). Although the correlation coefficient between SCF and RAF is approximately 0.1, the confidence level is low (P=0.3). The obvious seasonal variations of SCF over this region are mainly dominated by meteorological parameters. Their correlation coefficients are 0.61, 0.67 and 0.71 for skin temperature, vertical velocity and relative humidity, respectively. The third region is located over the southern ocean (80 ° E-90 ℃E, 50 ℃S-60 ℃S), where the maximum RAF of aerosol at the -20 ℃ isotherm can reach 0.07 (see Fig.10). Skin temperature and LTSS have negative correlations with SCF (-0.47 and -0.51, respectively), whereas a positive temporal correlation exists between SCF and U wind (approximately 0.44). These statistical results further indicate that the same meteorological parameter has a distinct effect in different regions on the variation of SCFs.

3.3 Spatial Correlations between SCFs and meteorological parameters

In this section, we further show that spatial correlations also exist between SCF and the meteorological parameters. To separate and quantify the meteorological factors of different latitudinal bands of SCFs under different aerosol loadings, we select three meteorological factors in the tropics (30 ℃N-30 ℃S) and middle-high latitudes (90 ℃N-40 ℃N; 40 ℃S-90 ℃S). Then, each meteorological factor of grids is grouped into six bins based on its values within a specified aerosol loading level. In the current study, the aerosol loadings are divided into three levels based on relative aerosol frequencies. However, in view of the apparent difference of aerosol loading level between the tropics and middle-high latitudes, different thresholds are used. For the tropics, selected meteorological factors include vertical velocity at 500 hPa, relative humidity and skin temperature. Aerosol levels include: high level (RAF>0.05), middle level (0<RAF<0.05) and low level (RAF=0). For middle-high latitudes, LTSS, u wind at 100 hPa and skin temperature are used; the three aerosol levels are high level (RAF>0.1), middle level (0.01<RAF<0.1) and low level (RAF<0.01). Such grouping ensures a sufficient number of samples available in each bin (at least

hundreds of samples in each bin) to satisfy statistical significance. Moreover, note again that only regions with temporal correlations between SCFs and meteorological parameters at the 95% confidence level are used to calculate the spatial correlations between SCFs and meteorological parameters.

Fig. 11 shows clearly that different spatial correlations exist between SCF at the -20 ℃ isotherm and the meteorological parameters for different latitudes. The error bars correspond to the ±5 standard error. Here, the standard error (SE) is computed as: $SE = SD/\sqrt{N}$, where SD is the standard deviation of the data falling in a meteorological parameter bin (e.g., vertical velocity <-20 hPa/day) and aerosol loading level; N is the sample number in each bin. At a fixed isotherm (such as, -20 ℃) for the tropics, we may find that SCFs and 500-hPa vertical velocity (or relative humidity at 500 hPa) have a significant positive correlation spatially significantly at the 95% confidence level for all aerosol loadings. However, the low correlations and confidence level (large p value) in Fig. 11c verify that the obvious spatial correlation vanishes for skin temperature. Moreover, we also note that no evident correlation exists between SCFs and aerosol loading levels under the same meteorological conditions in the tropics. By performing a similar analysis at different isotherms, we confirm this conclusion. The spatial correlation coefficients between SCFs and meteorological parameters at the -10 ℃ and -30 ℃ isotherms are summarized in Table 1. The statistical results thus indicate that the changes of tropical SCFs at a given isotherm are mainly controlled by the meteorological parameters, especially vertical velocity and relative humidity. However, the significance level of their spatial correlations decreases with decreasing temperature, especially at -30 ℃ isotherms (see Table 1). For the middle-high latitude, however, the obvious spatial correlations mainly exist between SCFs and U wind at 100 hPa and skin temperature. In summary, strong horizontal wind and low skin temperature tend to inhibit the glaciation of supercooled droplets. Moreover, high aerosol loading corresponds to SCFs calculated by using CALIOP retrievals, which are relatively low. This result is consistent with the previous study of Tan et al. (2014), which demonstrated that SCFs and RAFs of

dust, polluted dust and smoke are not only temporally negatively correlated but also spatially negatively correlated. Compared with horizontal wind and skin temperature, the spatial correlation between SCFs at the -20℃ isotherm and LTSS has a "U"-pattern; thus, there is no monotonous tendency (see Fig. 11d). Based on Fig. 5, the negative part of the correlation possibly corresponds to ocean regions, whereas the positive part of the correlation mainly corresponds to land regions (such as Siberia and America). From Table 1, we can see that positive spatial correlations between SCFs and u wind can be found almost at all isotherms and aerosol levels, whereas the impact of LTSS on the SCFs is regional because of obvious different correlations and weak significance level. Here, we emphasize that the statistical relationships between SCFs and meteorological parameters are based on the long- time (96 months) datasets, their temporal and spatial correlations at the 95% confidence level imply that it is very unlikely that the correlations happened by chance. Present study still can't give a quantitative conclusion to verify which parameter dominates the variation of SCFs at high dust loading regions (such as, northwest part of China). But, at least, it is certain that meteorological parameters dominate the variation of SCFs at a given isotherm for those clear regions, and their impacts depend on regions.

4. Conclusions and Discussion

Changes in cloud phase can significantly affect the Earth's radiation budget and global hydrological cycle. Based on the 8 years (2007-2015) of data of cloud phase information from CALIPSO-GOCCP, aerosol products from CALIPSO, and meteorological parameters from the ERA-Interim products, this study investigates the effects of atmospheric dynamics on the supercooled liquid cloud fraction under different aerosol loadings at a global scale. Although some statistical results reasonably agree with previous research, new insights are also achieved in this paper.

Previous studies have mainly focused on warm water cloud systems (Li et al., 2011, 2013; Kawamoto and Suzuki, 2012, 2013) or dust properties retrieval and simulations (Huang et al., 2010; Bi et al., 2011; Liu et al., 2011; Chen et al., 2013) or have demonstrated the importance of dust with respect to cloud properties (Huang et al., 2006b, 2006c, 2014; Su et al., 2008; Wang et al., 2010; 2015; 2016). Some studies

have investigated the impact of different aerosol types on cold phase clouds over East Asia (Zhang et al., 2015) or at a global scale (Choi et al., 2010; Tan et al., 2014). However, systematic studies of the statistical relationship between cloud phase changes and meteorological parameters at a global scale have received far less attention. To clarify the roles of different meteorological factors in determining cloud phase changes and further provide observational evidence for the design and evaluation of a more physically based cloud phase partitioning scheme, we perform temporal and spatial correlations between SCFs and different meteorological factors. Only values of those regions with temporal correlations between SCFs and meteorological parameters at the 95% confidence level are used to determine spatial correlation.

Statistical results indicate that aerosols' effect on nucleation cannot fully explain all SCF changes, especially in those regions where aerosols' effect on nucleation is not a first-order influence (e.g., due to low IN aerosol frequency). We find that the impacts of different meteorological factors on SCFs contain obvious regional differences. In the tropics, obvious positive correlations between SCFs and vertical velocity and relative humidity indicate that high vertical velocity and relative humidity suppress ice formation. However, the impacts of LTSS, skin temperature and horizontal wind on SCFs are relatively complex than those of vertical velocity and humidity. Their temporal correlations with SCFs depend on latitude or surface type. For example, at the -10℃ isotherm, negative temporal correlations for skin temperature are mainly located in Europe and ocean regions between 30° and 60° for two hemispheres, whereas positive correlations can be found in the tropics, Mainland China and Greenland.. However, with decreasing temperature (e.g., at the -20 ℃ isotherm), temporal correlation coefficients between SCFs and skin temperature are almost negative in middle and high latitudes. However, it is clear that the temporal correlations between SCFs and different meteorological parameters also gradually weaken (even vanish) with decreasing temperature. By analyzing the spatial correlations between SCFs and meteorology under different aerosol loadings, we find that positive spatial correlations also exist between SCF and the vertical velocity and

humidity in the tropics, whereas no evident correlation exists between SCFs and aerosol loading levels under the same meteorological conditions in the tropics. At middle and high latitudes, the obvious positive (or negative) spatial correlations mainly exist between SCFs and u wind at 100hPa (or skin temperature).This result indicates that strong horizontal wind and low skin temperature tend to inhibit the glaciation of supercooled droplets. Recently, there is evidence has shown that a cloud phase feedback occurs, causing more shortwave to be reflected back out to space relative to the state prior to global warming (McCoy et al., 2014; 2015). Our results, which are based on long- times' (96 months) global observations verify the effects of dynamic factors on cloud phase changes and illustrate that these effects are regional, thus suggesting potential implications for further reducing the biases of climate feedbacks and climate sensitivity among climate models.

Acknowledgments.

This research was jointly supported by the key Program of the National Natural Science Foundation of China (41430425), Foundation for Innovative Research Groups of the National Science Foundation of China (Grant No. 41521004), National Science Foundation of China (Grant No. 41575015 and 41205015) and the China 111 project (No. B13045). We would like to thank the CALIPSO-GOCCP, CALIPSO and ERA-Interim science teams for providing excellent and accessible data products that made this study possible.

References

Andrews, T., Gregory, J. M., Webb, M. J., and Taylor, K. E.: Forcing, feedbacks and climate sensitivity in CMIP5 coupled atmosphere–ocean climate models, Geophys. Res. Lett., 39, L09712, doi:10.1029/2012GL051607, 2012.

Atkinson, J. D., Murray, B. J., Woodhouse, M. T., et al.: The importance of feldspar for ice nucleation by mineral dust in mixed-phase clouds, Nature, 498, 355-358, 2013.

Bergeron, T.,: On the physics of cloud and precipitation, Proc. Fifth Assembly UGGI Lisbon, Vol. 2, Lisbon, Portugal, UGGI, 156–173, 1935.

Bey, I., Jacob, D. J., Yantosca, R. M., Logan, J. A., Field, B. D., Fiore, A. M., Li, Q., Liu, H. Y., Mickley, L. J., and Schultz, M. G.: Global modeling of tropospheric chemistry with assimilated meteorology: Model description and evaluation, J. Geophys. Res., 106(D19), 23, 073–23,095, doi:10.1029/2001JD000807, 2001.

Bi J., Huang, J., Fu, Q., Wang, X., Shi, J., Zhang, W., Huang, Z., and Zhang, B.: Toward characterization of the aerosol optical properties over Loess Plateau of Northwestern China, J. Quant. Spectrosc. Radiat. Transf., 112, D00K17, doi:10.1029/2009JD013372, 2011.

Borovikov, A. M., Gaivoronskii, I. I., Zak, E. G., Kostarev, V. V., Mazin, I. P., Minervin, V. E., Khrgian. A. Kh. and Shmeter, S. M. 'Clouds physics'. Israel Program for Scientific Translation. Available from US Dept. of Commerce, Washington, DC, USA,1963.

Bower, K. N., Moss, S. J., Johnson, D.W., Choularton, T.W., Latham, J., Brown, P. R. A., Blyth, A.M., and Cardwell, J.: A parameterization of the ice water content observed in frontal and convective clouds, Quart. J. Roy. Meteor. Soc., 122, 1815–1844, 1996.

Bodas-Salcedo, A, et al.: COSP: Satellite simulation software for model assessment, Bull. Am. Meteorol. Soc., 92, 1023–1043, doi:10.1175/ 2011BAMS2856, 2011.

Ceccaldi, M., Delano ¨e, J., Hogan, R. J., Pounder, N. L., Protat, A., and Pelon, J.: From CloudSat-CALIPSO to EarthCare: Evolution of the DARDAR cloud classification and its comparison to airborne radar-lidar observations, J. Geophys. Res., 118(14), 7962–7981, doi:10.1002/jgrd.50579, 2013.

Cesana, G., Kay, J. E., Chepfer, H., English, J. M., and deBoer G.: Ubiquitous low-level liquid-containing Arctic clouds: New observations and climate model constraints from CALIPSO-GOCCP, Geophys. Res. Lett., 39, L20804, doi:10.1029/2012GL053385, 2012.

Cesana, G., and Chepfer, H.: Evaluation of the cloud water phase in a climatemodel using CALIPSO-GOCCP, J. Geophys. Res. Atmos, 118, 7922–7937,

doi:10.1002/jgrd.50376, 2013.

Cesana, G., Waliser, D. E., Jiang, X., and Li, J.-L. F.: Multi-model evaluation of cloud phase transition using satellite and reanalysis data, J. Geophys. Res. Atmos., 120, 7871–7892, doi:10.1002/2014JD022932, 2015.

Chen, S., Huang, J., Zhao, C., Qian, Y., Leung, R., and Yang, B.: Modeling the transport and radiative forcing of Taklimakan dust over the Tibetan Plateau: A case study in the summer of 2006, J. Geophys. Res., 118, doi:10.1002/jgrd.50122, 2013.

Cheng, A., Xu, K.M., Hu, Y., and Kato, S.: Impact of a cloud thermodynamic phase parameterization based on CALIPSO observations on climate simulation, J. Geophys. Res., 117, D09103, doi:10.1029/2011JD017263, 2012.

Chepfer, H., Bony, S., Winker, D. M., Chiriaco, M., Dufresne, J.-L., and Seze, G.: Use of CALIPSO lidar observations to evaluate the cloudiness simulated by a climate model, Geophys. Res. Lett., 35, L15704, doi:10.1029/2008GL034207, 2008.

Chepfer, H., Bony, S., Winker, D., Cesana, G., Dufresne, J. L., Minnis, P., Stubenrauch, C. J., and Zeng, S.: The GCM Oriented Calipso Cloud Product (CALIPSO-GOCCP), J. Geophys. Res., 115, D00H16, doi:10.1029/2009JD012251, 2010.

Choi, Y.S., Lindzen, R.S., Ho, C.H., and Kim, J.: Space observations of cold-cloud phase change, Proc. Natl. Acad. Sci. U.S.A., 107, 11, 211–11,216, 2010.

Cziczo, D.J., Froyd, K.D., Hoose, C., Jensen, E.J., Diao, M., Zondlo, M.A., Smith, J.B., Twohy, C.H., and Murphy, D.M.: Clarifying the dominant sources and mechanisms of cirrus cloud formation, Science, 340(6138), 1320–1324, doi:10.1126/science.1234145, 2013.

Dee, D.P., Uppala, S.M., Simmons, A.J., et al.: The ERA‐Interim reanalysis: Configuration and performance of the data assimilation system, Quart. J. Roy. Meteor. Soc., 137(656), 553-597, 2011.

Delanoe, J., and Hogan R. J.: Combined CloudSat–CALIPSO–MODIS retrievals of the properties of ice clouds, Journal of Geophysical Research–Atmospheres, 115,

D00H29, doi:10.1029/2009JD012346, 2010.

DeMott, P.J., Prenni, A.J., Liu, X., et al.: Predicting global atmospheric ice nuclei distributions and their impacts on climate, Proc. Natl. Acad. Sci. U. S. A., 107(25), 11217-11222, 2010.

Forbes, R.M., and Ahlgrimn, M.: On the Representation of High-Latitude Boundary Layer Mixed-Phase Cloud in the ECMWF Global Model, Mon. Weather Rev.,142, 3425-3445, DOI: 10.1175/MWR-D-13-00325.1, 2014.

Findeisen, W.: The evaporation of cloud and raindrops, Meteor. Z., 56, 453–460, 1939.

Fu, Q.: A new parameterization of an asymmetry factor of cirrus clouds for climate models.J. Atmos. Sci., 64, 4144-4154, 2007.

Fu, Q., Sun, W.B., and Yang, P.: On modeling of scattering and absorption by nonspherical cirrus ice particles in thermal infrared wavelengths, J. Atmos. Sci., 56, 2937-2947, 1999.

Giraud, V., Thouron, O., Riedi, J., and Goloub, P.: Analysis of direct comparison of cloud top temperature and infrared split window signature against independent retrievals of cloud thermodynamic phase, Geophys. Res. Lett., 28, 983–986, 2001.

Hogan, R.J., Illingworth, A.J., O'Connor, E.J., and Poiares Baptista, J.P.V.: Characteristics of mixed-phase clouds. II: A climatology from ground-based lidar, Quart. J. Roy. Meteor. Soc., 129, 2117–2134, 2003.

Hu, Y., Vaughan, M., Liu, Z., Lin, B., Yang, P., Flittner, D., Hunt, W., Kuehn, R., Huang, J., Wu, D., Rodier, S., Powell, K., Trepte, C., and Winker, D.: The depolarization-attenuated backscatter relation: CALIPSO lidar measurements vs. theory, Opt. Exp., 15, 5327–5332, 2007.

Hu, Y., Winker, D., Vaughan, M., Lin, B., Omar, A., Trepte, C., Flittner, D., Yang, P., Nasiri, S., Baum, B. A., Sun, W., Liu, Z., Wang, Z., Young, S., Stamnes, K., Huang, J., Kuehn, R., and Holz, R. E.: CALIPSO/ CALIOP cloud phase discrimination algorithm, J. Atmos. Ocean. Technol., 26, 2206–2309. DOI:10.1175/2009JTECHA1280.1, 2009.

Hu, Y., Rodier, S., Xu, K.M., Sun,W., Huang, J., Lin, B., Zhai, P., and Josset, D.: Occurrence, liquid water content, and fraction of supercooled water clouds from combined CALIOP/IIR/MODIS measurements, J. Geophys. Res., 115, D00H34, doi:10.1029/2009JD012384, 2010.

Huang, J. P., Minnis, P., and Lin, B.: Advanced retrievals of multilayered cloud properties using multispectral measurements, J. Geophys. Res., 110, D15S18, doi:10.1029/2004JD005101, 2005.

Huang, J. P., Minnis, P., and Lin, B.: Determination of ice water path in ice-over-water cloud systems using combined MODIS and AMSR-E measurements, Geophys. Res. Lett., 33, L21801, doi:10.1029/ 2006GL027038, 2006a.

Huang, J.P., Lin, B., Minnis, P., Wang, T., Wang, X., Hu, Y., Yi, Y., and Ayers, J.R.: Satellite-based assessment of possible dust aerosols semi-direct effect on cloud water path over East Asia, Geophys. Res. Lett., 33, L19802, doi: 10.1029/2006GL026561, 2006b.

Huang, J.P., Minnis, P., Lin, B., Wang, T., Yi, Y., Hu, Y., Sun-Mack, S., and Ayers, K.: Possible influences of Asian dust aerosols on cloud properties and radiative forcing observed from MODIS and CERES, Geophys. Res. Lett., 33, L06824, doi: 10.1029/2005GL024724, 2006c.

Huang, J.P., Minnis, P., Chen, B., Huang, Z., Liu, Z., Zhao, Q., Yi, Y., and Ayers, J. K.: Long-range transport and vertical structure of Asian dust from CALIPSO and surface measurements during PACDEX, *J. Geophys. Res.*, *113*, D23212, doi:10.1029/2008JD010620, 2008.

Huang, J.P., Wang, T., Wang, W., Li, Z., and Yan, H.: Climate effects of dust aerosols over East Asian arid and semiarid regions, J. Geophys. Res., 119, 11398–11416, doi:10.1002/2014JD021796, 2014.

Huang, Z., Huang, J., Bi, J., Wang, G., Wang, W., Fu, Q., Li, Z., Tsay, S.-C., and Shi, J.: Dust aerosol vertical structure measurements using three MPL lidars during 2008 China-U.S. joint dust field experiment, J. Geophys. Res., 115 D00K15, doi:10.1029/2009JD013273, 2010.

Intrieri, J.M., Shupe, M.D., Uttal, T., and McCarty, B.J.: An annual cycle of Arctic

cloud characteristics observed by radar and lidar at SHEBA, J. Geophys. Res., 107, 8030, doi:10.1029/2000JC000423, 2002.

Kawamoto, K., Suzuki, K.: Microphysical transition in water clouds Over the Amazon and China derived from space-borne radar and Radiometer data, J. Geophys. Res., 117, D05212. http://dx.doi.org/10.1029/2011JD016412, 2012.

Kawamoto, K., Suzuki, K.: Comparison of water cloud microphysics over mid-latitude land and ocean using CloudSat and MODIS observations, J. Quant. Spectrosc. Radiat. Transf., 122, 13–24, 2013.

Klein, S. A. and Hartmann, D. L.: The seasonal cycle of low stratiform clouds, J. Clim., 6, 1588–1606, 1993.

Korolev, A. V., Isaac, G. A., Cober, S. G., Strapp, J. W., and Hallett, J.: Microphysical characterization of mixed-phase clouds, Q. J. R. Meteorol. Soc., 129, 39–65, doi:10.1256/qj.01.204, 2003.

Li, J., Yi, Y., Minnis, P., Huang, J., Yan, H., Ma, Y., Wang, W., Ayers, J. K.: Radiative effect differences between multi-layered and single-layer clouds derived from CERES, CALIPSO, and CloudSat data, J. Quant. Spectrosc. Radiat. Transf., 112, doi:10.1016/j.jqsrt.2010.10.006, 2010.

Li, J., Hu, Y., Huang, J., Stamnes, K., Yi, Y., and Stamnes, S.: A new method for retrieval of the extinction coefficient of water clouds by using the tail of the CALIOP signal, Atmos. Chem. Phys., 11, 1-15, 2011.

Li, J., Yi, Y. H., Stamnes, K., Ding, X. D., Wang, T. H., Jin, H. C., and Wang, S. S.: A new approach to retrieve cloud base height of marine boundary layer clouds, Geophys. Res. Lett., 40, 4448–4453, doi:10.1002/grl.50836, 2013.

Li, J., Huang, J., Stamnes, K., Wang, T., Lv, Q., and Jin, H.: A global survey of cloud overlap based on CALIPSO and CloudSat measurements, Atmos. Chem. Phys., 15, 519-536, doi:10.5194/acp-15-519-2015, 2015.

Liu, Y., Huang, J., Shi, G., Takamura, T., Khatri, P., Bi, J., Shi, J.,Wang, T., Wang, X., and Zhang, B.: Aerosol optical properties and radiative effect determined from sky-radiometer over Loess Plateau of Northwest China, Atmos. Chem. Phys., 11, 11455–11463, doi:10.5194/acp-11-11455-2011, 2011.

Liu, Z., Vaughan, M., Winker, D., Kittaka, C., Getzewich, B., Kuehn, R., Omar, A., Powell, K., Trepte, C., and Hostetler, C.:The CALIPSO lidar cloud and aerosol discrimination: Version 2 algorithm and initial assessment of performance, J. Atmos. Oceanic Technol., 26(7), 1198–1213, doi:10.1175/2009JTECHA1229.1, 2009.

Lv, Q., Li, J., Wang, T., and Huang, J.: Cloud radiative forcing induced by layered clouds and associated impact on the atmospheric heating rate, J. Meteor. Res., 29(5), 779-792, doi: 10.1007/s13351-015-5078-7, 2015.

McCoy, D.T., Hartmann, D. L., and Grosvenor, D.P.: Observed Southern Ocean Cloud Properties and Shortwave Reflection Part 2: Phase changes and low cloud feedback, J. Climate, 27, 8858-8868, doi:10.11175/JCLI-D-14-00288.1, 2014.

McCoy, D.T., Hartmann, D. L., Zelinka, M.D., Ceppi, P., and Grosvenor, D.P.: Mixed-phase cloud physics and Southern Ocean cloud feedback in climate models, J. Geophys. Res. Atmos., doi: 10.1002/2015JD023603, 9539-9554, 2015.

Mielonen, T., Arola, A., Komppula, M., Kukkonen, J., Koskinen, J., Leeuw, G. de., and Lehtinen, K. E. J.: Comparison of CALIOP level 2 aerosol subtypes to aerosol types derived from AERONET inversion data, Geophys. Res. Lett., 36, L18804, doi:10.1029/2009GL039609, 2009.

Morrison, A. E, Siems, S.T, and Manton, M. J.: A three-year climatology of cloud-top phase over the Southern Ocean and North Pacific, J. Clim., 24(9), 2405-2418, 2011.

Mülmenstädt, J., O. Sourdeval,J. Delanoë, and J. Quaas (2015), Frequency of occurrence of rain from liquid-, mixed-, and ice-phase clouds derived from A-Train satellite retrievals, Geophys. Res. Lett., 42, 6502–6509, doi:10.1002/2015GL064604.

Naud, C.M., Del Genio, A.D., and Bauer, M.: Observational constraints on the cloud thermodynamic phase in midlatitude storms, J. Clim., 19(20), 5273-5288, 2006.

Niedermeier, D., et al.: Experimental study of the role of physicochemical surface processing on the IN ability of mineral dust particles, Atmos. Chem. Phys.,

11(21), 11,131–11,144, doi:10.5194/acp-11-11131-2011, 2011.

Noel, V., and Chepfer, H.: A global view of horizontally oriented crystals in ice clouds from Cloud‐Aerosol Lidar and Infrared Pathfinder Satellite Observation (CALIPSO), J. Geophys. Res., 115, D00H23, doi:10.1029/2009JD012365, 2010.

Omar, A. H., et al.: The CALIPSO automated aerosol classification and lidar ratio selection algorithm, J. Atmos. Oceanic Technol., 26(10), 1994–2014, doi:10.1175/2009JTECHA1231.1, 2009.

Pruppacher, H. R., and Klett, J. D.:Microphysics of Clouds and Precipitation, 2nd ed., 954 pp., Kluwer Acad., Dordrecht, Netherlands, 1997.

Richardson, M. S., et al.: Measurements of heterogeneous ice nuclei in the western United States in springtime and their relation to aerosol characteristics, J. Geophys. Res., 112, D02209, doi:10.1029/2006JD007500, 2007.

Sassen, K.: Evidence of liquid phase cirrus cloud formation from volcanic aerosols: Climate implications, Science, 257, 516–519, 1992.

Sassen, K., and Khvorostyanov, V.I.: Microphysical and radiative properties of mixed phase altocumulus: a model evaluation of glaciation effects. Atmos. Res., 84, 390–398, 2007.

Shupe, M.D., Matrosov, S.Y., and Uttal, T.: Arctic mixed-phase cloud properties derived from surface-based sensors at SHEBA, J. Atmos. Sci., 63(2), 697-711, 2006.

Stephens, G.L., Vane, D.G., Boain, R.J., Mace, G.G., Sassen, K., Wang, Z., Illingworth, A.J., O'Connor, E.J., Rossow, W.B., Durden, S.L., Miller, S.D., Austin, R.T., Benedetti, A., Mitrescu, C., and CloudSat Science Team.: The CloudSat mission and the A-Train, A new dimension of space-based observations of clouds and precipitation, B. Am. Meteorol. Soc., 83, 1771–1790, 2002.

Su, J., Huang, J., Fu, Q., Minnis, P., Ge, J., and Bi, J.: Estimation of Asian dust aerosol effect on cloud radiation forcing using Fu-Liou radiative model and CERES measurements, Atmos. Chem. Phys., 8, 2763-2771, 2008.

Sun, W.B., Loeb, N., Videen, G., Fu, Q.: Examination of surface roughness on light

scattering by long ice columns by use of a two-dimensional finite-difference time-domian algorithm, Appl. Opt., 43, 1957 – 1964, 2004.

Sun, W., Baize, R. R., Videen, G., Hu, Y., and Fu, Q.: A method to retrieve super-thin cloud optical depth over ocean background with polarized sunlight, Atmos. Chem. Phys., 15, 11909-11918, doi:10.5194/ acp-15-11909-2015, 2015.

Tan, I., Storelvmo, T., and Choi, Y.S.: Spaceborne lidar observations of the ice-nucleating potential of dust, polluted dust and smoke aerosols in mixed-phase clouds, J. Geophys. Res. Atmos., 119, 6653–6665, doi:10.1002/2013JD021333, 2014.

Taylor, K. E., Stouffer, R. J., and Meehl G. A.: An overview of CMIP5 and the experiment design, Bull. Am. Meteorol. Soc., 93, 485–498, doi:10.1175/BAMS-D-11-00094.1, 2012.

Tsushima, Y., Emori, S., Ogura, T., Kimoto, M., Webb, M. J., Williams, K. D., Ringer, M. A., Soden, B. J., Li, B., and Andronova, N.: Importance of the mixed phase cloud distribution in the control climate for assessing the response of clouds to carbon dioxide increase: a multi‐model study, Clim. Dyn., 27, 113–126, 2006.

Wang, W., Huang, J., Minnis, P., Hu, Y., Li, J., Huang, Z., Ayers,J. K., and Wang, T.: Dusty cloud properties and radiative forcing over dust source and downwind regions derived from A-Train data during the Pacific Dust Experiment, J. Geophys. Res., 115, D00H35, doi:10.1029/2010JD014109, 2010.

Wang, W., Sheng, L., Jin, H., and Han. Y.: Dust Aerosol Effects on Cirrus and Altocumulus Clouds in Northwest China, J. Meteor. Res., 29 (5): 793-805, 2015.

Wang, W., Sheng, L., Dong, X., Qu, W., Sun, J., Jin, H., and Logan, T.: Dust aerosol impact on the retrieval of cloud top height from satellite observations of CALIPSO, CloudSat and MODIS, J. Quant. Spectrosc. Radiat. Transf., doi:10.1016/j.jqsrt.2016.03.034, 2016.

Wegener, A.: Thermodynamik der Atmosphäre. JA Barth, 331 pp, 1911.

West, R. E. L., Stier, P., Jones, A., Johnson, C. E., Mann, G. W., Bellouin, N., Partridge, D. G., and Kipling Z.: The importance of vertical velocity variability

for estimates of the indirect aerosol effects, Atmos. Chem. Phys., 14, 6369–6393, doi:10.5194/acp-14-6369-2014, 2014.

Winker D. M., Hunt, W. H., and Mcgill, M. J.: Initial performance assessment of CALIOP, Geophys. Res. Lett., 34, L19803, doi:10.1029/ 2007GL030135, 2007.

Wood, R.: Stratocumulus clouds, *Mon. Wea. Rev.*, 140, 2373-2423, 2012.

Yuan, T. and Oreopoulos, L.: On the global character of overlap between low and high clouds, Geophys. Res. Lett., 40, 5320–5326, doi:10.1002/grl.50871, 2013.

Yun,Y., and Penner, J.E.: Global model comparison of heterogeneous ice nucleation parameterizations in mixed phase clouds, J. Geophys. res., 117, D07203, doi:10:1029/2011JD016506, 2012.

Zhang, D., Wang, Z., and Liu D.: A global view of midlevel liquid-layer topped stratiform cloud distribution and phase partition from CALIPSO and CloudSat measurements, J. Geophys. Res., 115, D00H13, doi: 10.1029/2009JD012143, 2010.

Zhang, D., Liu, D., Luo, T., Wang, Z., and Yin, Y.: Aerosol impacts on cloud thermodynamic phase change over East Asia observed with CALIPSO and CloudSat measurements, J. Geophys. Res. Atmos., 120, 1490–1501, doi:10.1002/2014JD022630, 2015.

Table1. The summary of spatial correlation coefficients between SCFs and meteorological parameters at three isotherms under different aerosol loading conditions. Only regions with temporal correlations between SCFs and meteorological parameters at the 95% confidence level are used to calculate the spatial correlations between SCFs and meteorological parameters.

Isotherm(℃)		**-10**			**-20**			**-30**	
	HAL[a]	**MAL**[a]	**LAL**[a]	**HAL**	**MAL**	**LAL**	**HAL**	**MAL**	**LAL**
Velocity (tropics)	0.98	0.98	0.99	0.98	0.99	0.97	0.99	0.27	0.63
								P=0.6[b]	**P=0.2**
RH (tropics)	0.99	0.99	0.96	0.99	0.98	0.97	0.57	0.43	0.39
							P=0.23	**P=0.4**	**P=0.44**
ST (tropics)	0.21	0.57	-0.56	-0.08	-0.47	-0.78	NaN	-0.67	-0.99
	P=0.7	**P=0.24**	**P=0.25**	**P=0.88**	**P=0.34**	**P=0.06**		**P=0.15**	
U wind (middle Lat)	-0.95	0.95	0.79	0.98	0.99	0.92	0.83	0.99	0.95
LTSS (middle Lat)	-0.45	-0.62	-0.23	0.28	0.22	0.77	0.64	0.57	0.82
	P=0.37	**P=0.19**	**P=0.65**	**P=0.6**	**P=0.68**	**P=0.07**	**P=0.17**	**P=0.24**	
ST (middle Lat)	NaN	-0.7	-0.51	-0.93	-0.91	-0.93	-0.99	-0.92	-0.98
		P=0.13	**P=0.31**						

[a] HAL, MAL and LAL are represent the high, middle and low aerosol loading level; [b] We also provide the confidence value (i.e., p value) when the confidence level of the spatial correlation between variables is less than 95%.

Figure Captions

Fig.1. The global and seasonal variations of supercooled water cloud fractions (SCFs) and relative aerosol frequencies (RAFs) at -10 ℃ isotherm over 2 °×2 °grid boxes.

Fig.2. The global and seasonal variations of supercooled water cloud fractions (SCFs) and relative aerosol frequencies (RAFs) at -20 ℃ isotherm over 2 °×2 °grid boxes.

Fig.3. The global and seasonal variations of supercooled water cloud fractions (SCFs) and relative aerosol frequencies (RAFs) at -30 ℃ isotherm over 2 °×2 °grid boxes.

Fig.4. The zonal and seasonal variations of SCFs and RAFs at -20 ℃ isotherm.

Fig.5. Temporal correlations (at the 95% confidence level) between SCFs at three isotherms and skin temperature (left panel) and LTSS (right panel). The correlations are based on 96 months' monthly SCF and meteorological parameters. Grid size is: 10 °latitude by 10 °longitude.

Fig.6. Similar with Fig.5, but is for vertical velocity at 500 hPa (left panel) and relative humidity (right panel).

Fig.7. Similar with Fig.5, but is for u wind at 100 hPa.

Fig.8. Time series plots of SCFs, meteorological parameters and RAFs of IN aerosol at -30 ℃ isotherm over the central China (100 °E-110 °E, 30 °N-40 °N). Each line in every subplot corresponds to a time series of different variables after 5 months of smoothing. The coefficients (at the 95% confidence level) in subplots represent the temporal correlation between the original SCFs series and meteorological parameters (or RAFs). The confidence values (i.e., p value) are provided only when the confidence level of the temporal correlation between variables is less than 95%.

Fig.9. Similar with Fig.8, but is for -10 ℃ isotherm over a region near the Bahamas

(70 °W-60 °W, 20 °N-10 °N).

Fig.10. Similar with Fig.8, but is for -20 ℃ isotherm over the southern ocean (80 °E-90 °E, 50 °S-60 °S).

Fig.11. Spatial correlations between SCFs at -20 ℃ isotherm and meteorological parameters under different aerosol loading conditions. Left panel represents tropics, whereas right panel corresponds to the correlations in middle and high latitudes. Only those regions with temporal correlations between SCFs and meteorological parameters at the 95% confidence level are used to calculate the spatial correlations between SCFs and meteorological parameters. The confidence values (i.e., p value) are provided only when the confidence level of the spatial correlation between variables is less than 95%.

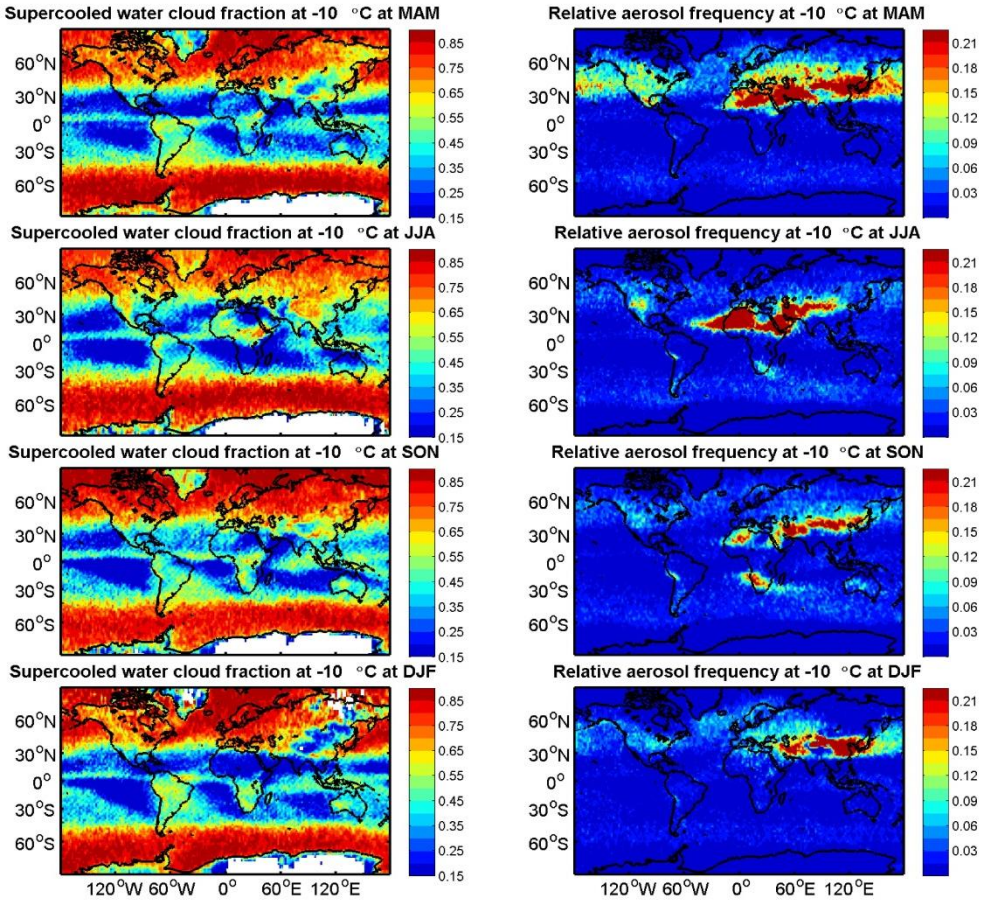

Fig.1. The global and seasonal variations of supercooled water cloud fractions (SCFs) and relative aerosol frequencies (RAFs) at -10 ℃ isotherm over 2 °×2 °grid boxes.

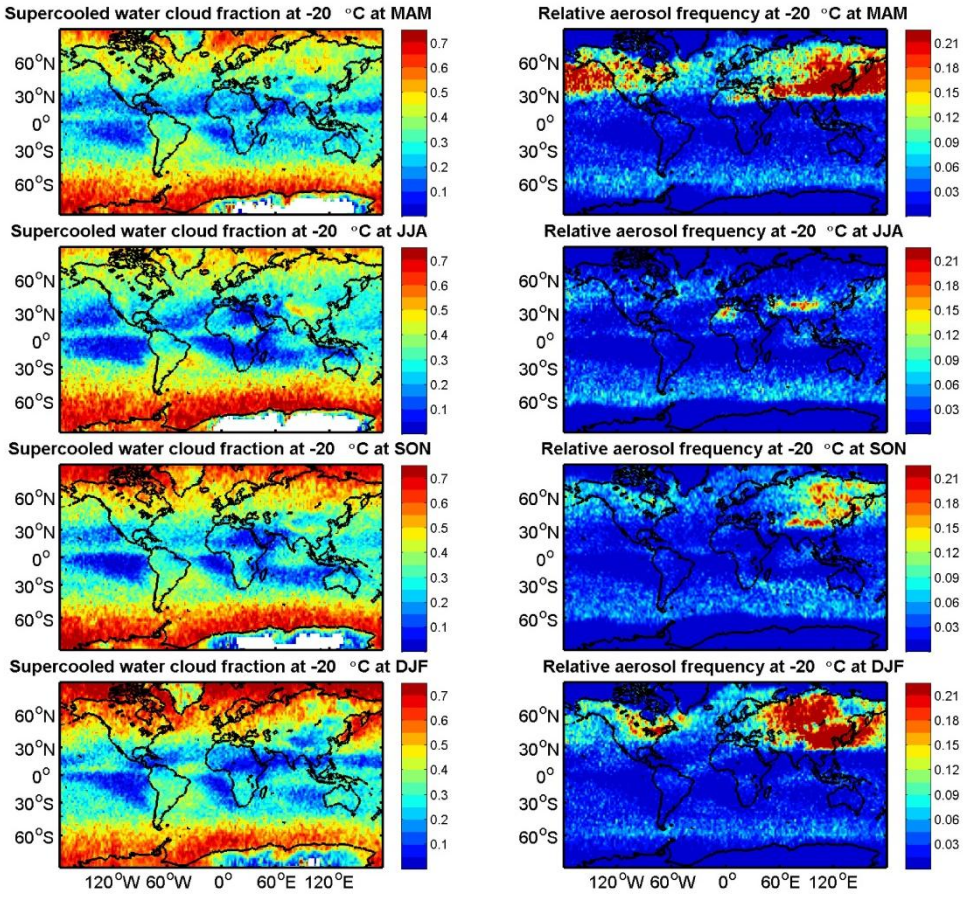

955 **Fig.2.** The global and seasonal variations of supercooled water cloud fractions (SCFs) and relative aerosol frequencies (RAFs) at -20 ℃ isotherm over 2 °×2 °grid boxes.

960

965

970

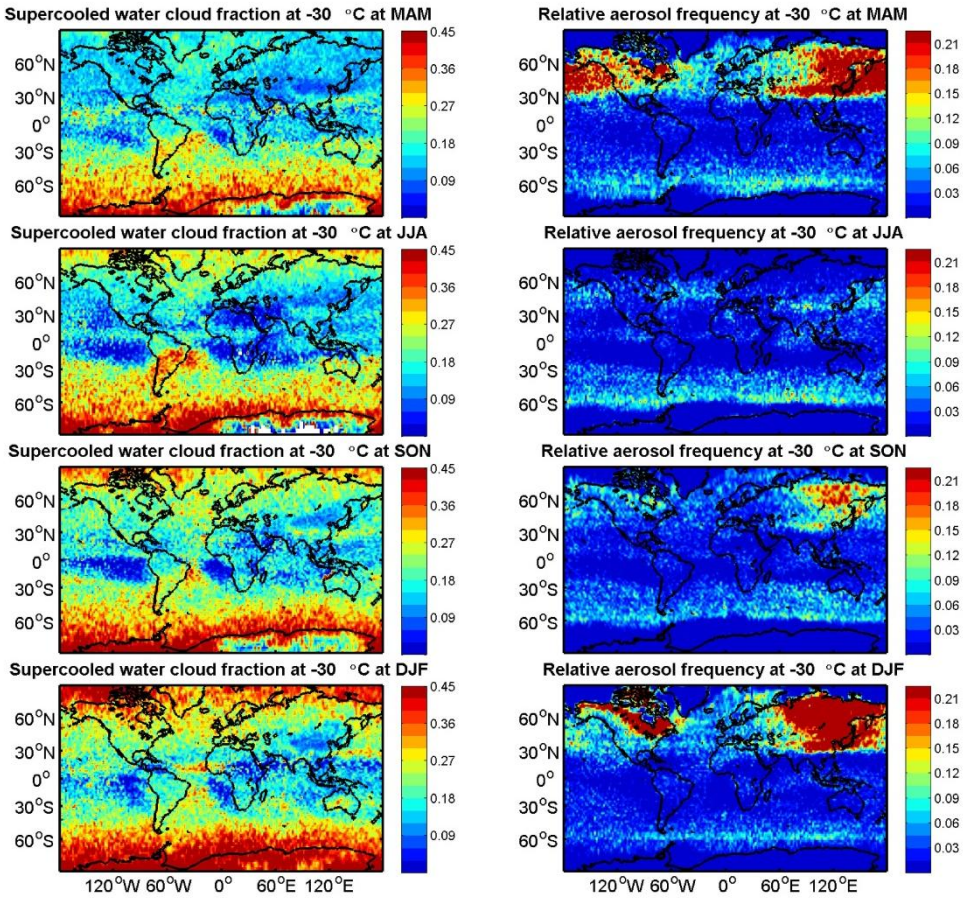

Fig.3. The global and seasonal variations of supercooled water cloud fractions (SCFs) and relative aerosol frequencies (RAFs) at -30 ℃ isotherm over 2 °×2 °grid boxes.

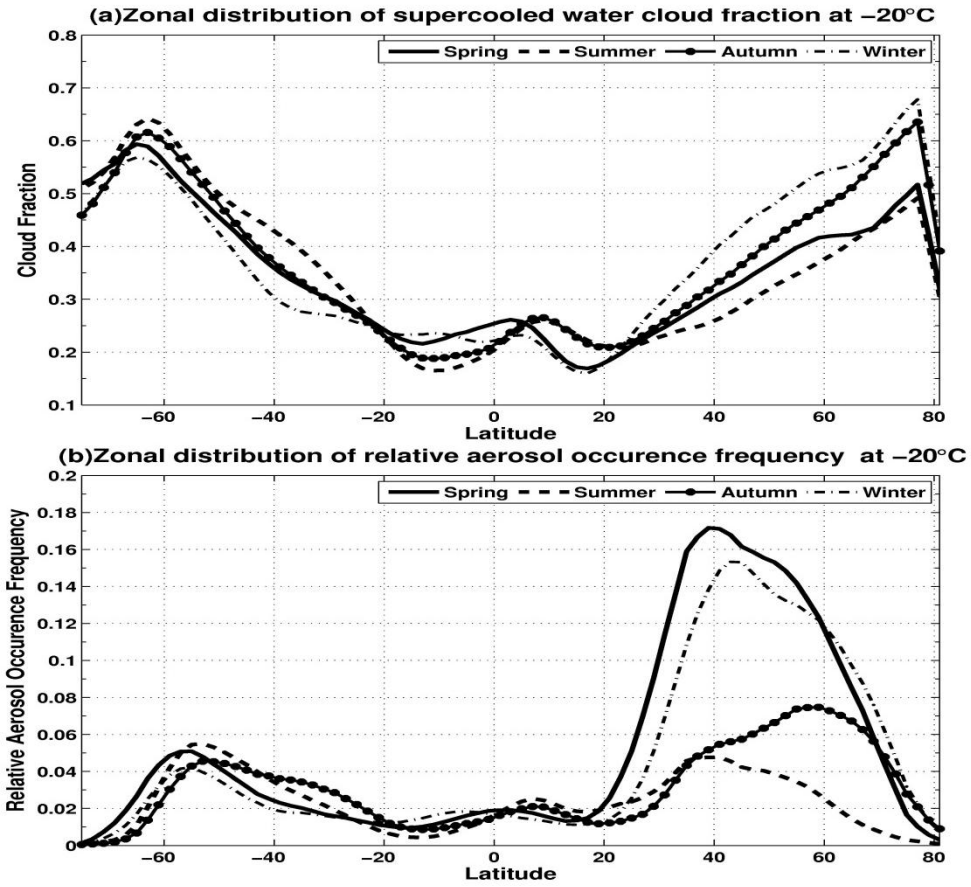

Fig.4. The zonal and seasonal variations of SCFs and RAFs at -20 ℃ isotherm.

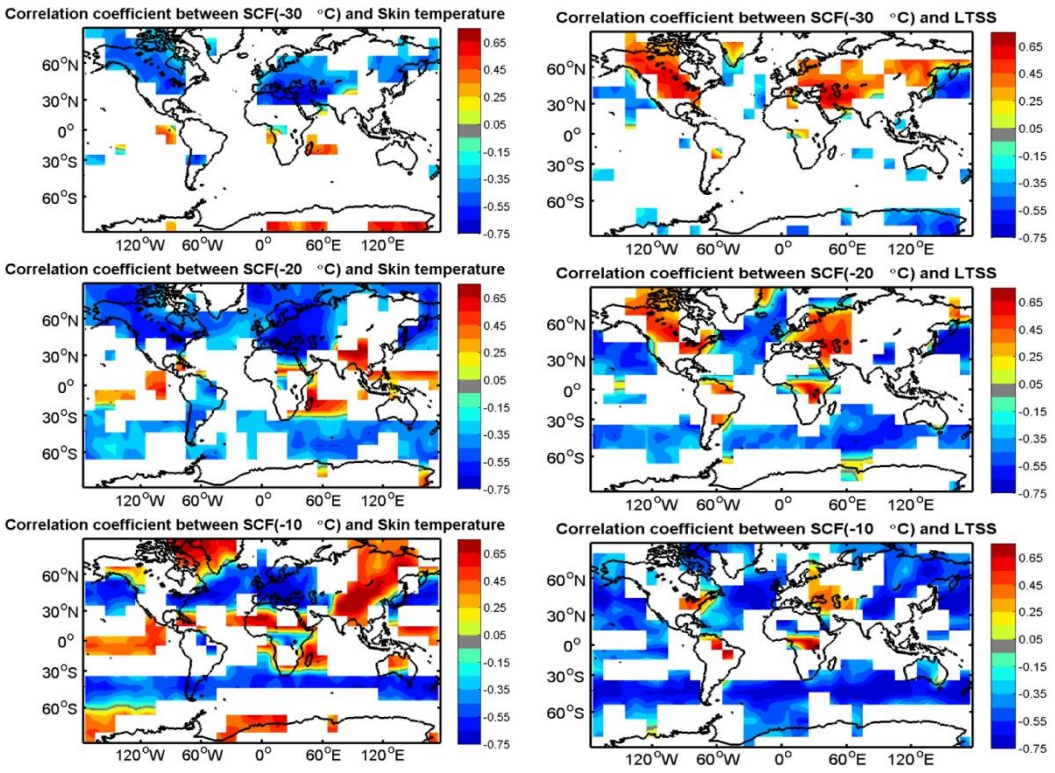

Fig.5. Temporal correlations (at the 95% confidence level) between SCFs at three isotherms and skin temperature (left panel) and LTSS (right panel). The correlations are based on 96 months' monthly SCF and meteorological parameters. Grid size is: 10 ºlatitude by 10 ºlongitude.

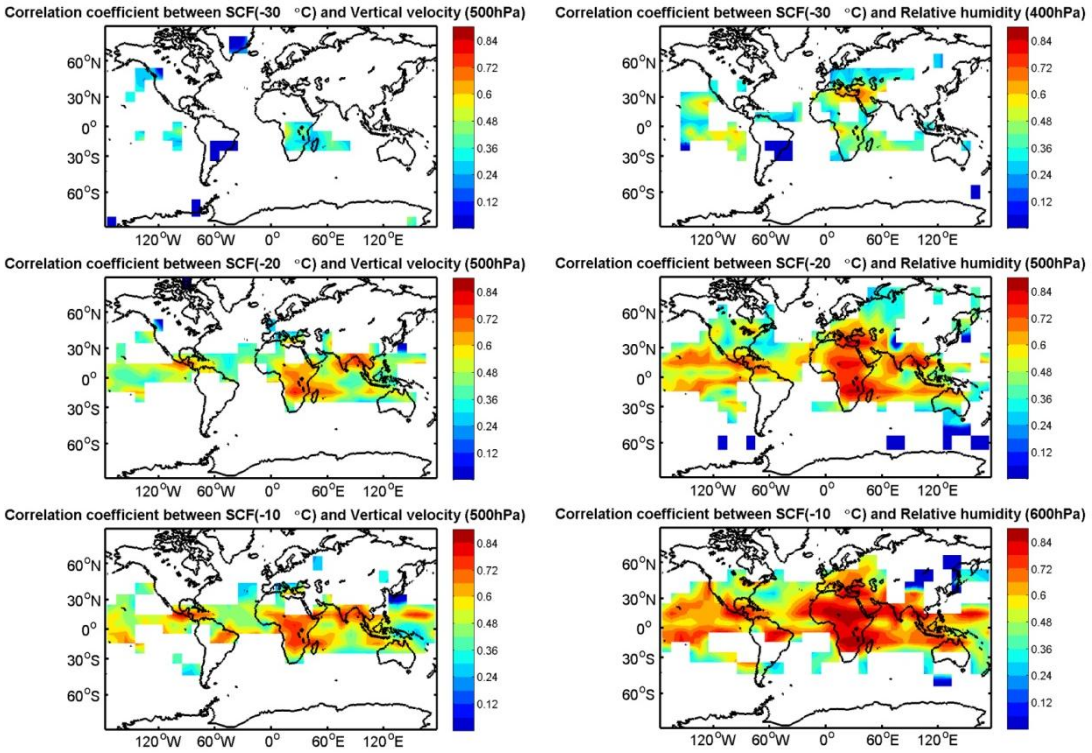

1045 **Fig.6.** Similar with Fig.5, but is for vertical velocity at 500 hPa (left panel) and relative humidity (right panel).

1050

1055

1060

1065

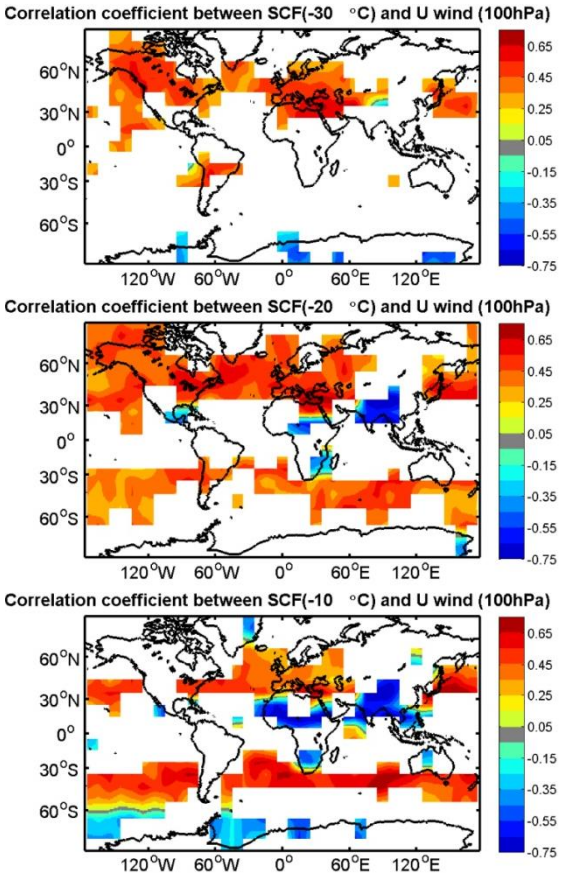

Fig.7. Similar with Fig.5, but is for u wind at 100 hPa.

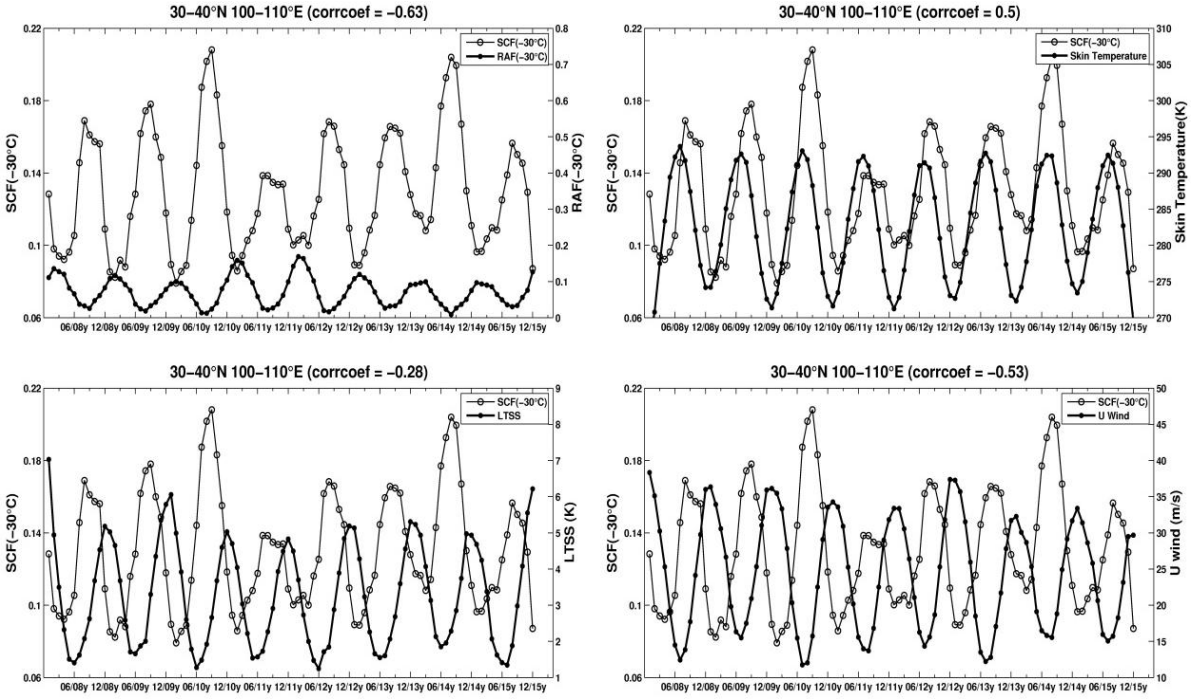

Fig.8. Time series plots of SCFs, meteorological parameters and RAFs of IN aerosol at -30 ℃ isotherm over the central China (100 ℃E-110 ℃E, 30 ℃N-40 ℃N). Each line in every subplot corresponds to a time series of different variables after 5 months of smoothing. The coefficients (at the 95% confidence level) in subplots represent the temporal correlation between the original SCFs series and meteorological parameters (or RAFs). The confidence values (i.e., p value) are provided only when the confidence level of the temporal correlation between variables is less than 95%.

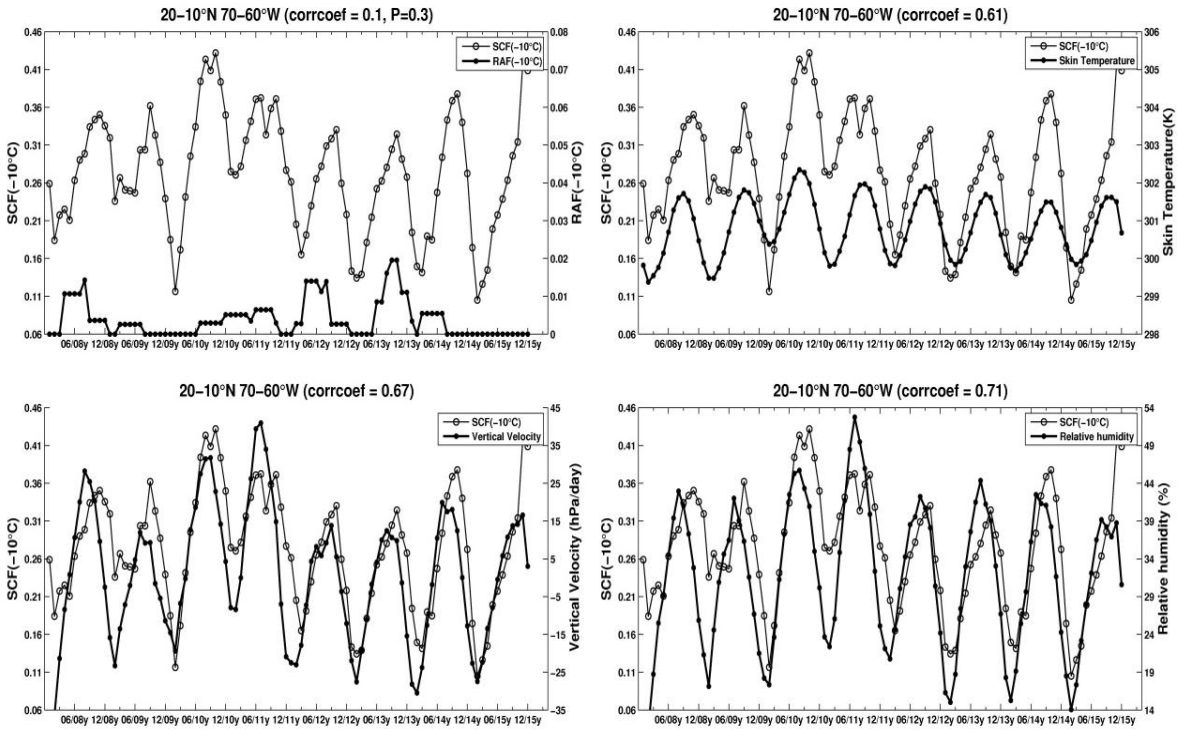

Fig.9. Similar with Fig.8, but is for -10 ℃ isotherm over a region near the Bahamas (70 ℃W-60 ℃W, 20 ℃N-10 ℃N).

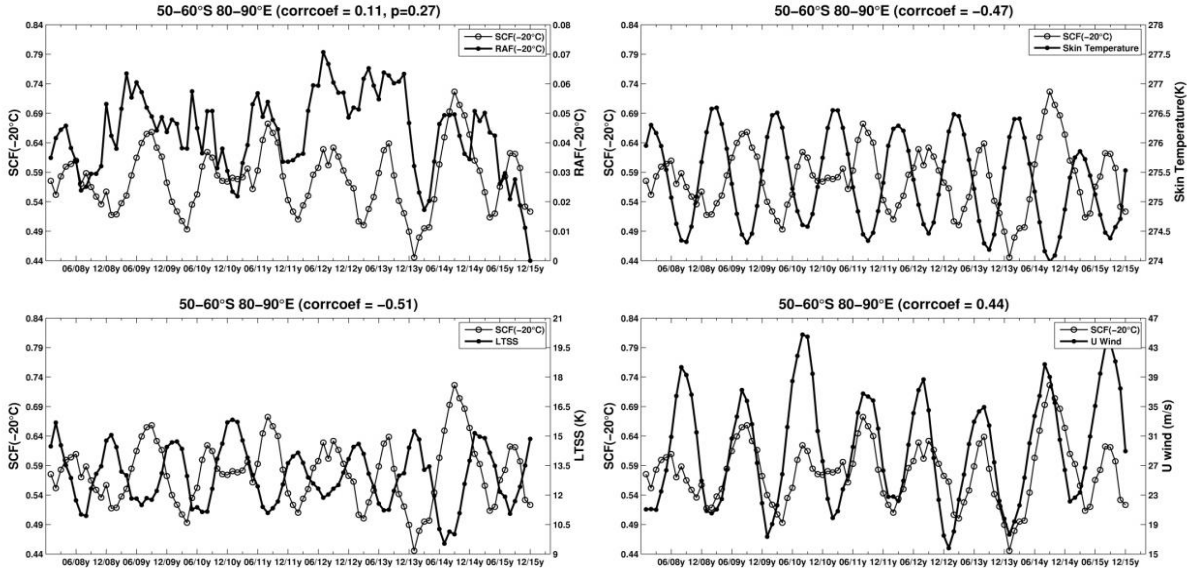

Fig.10. Similar with Fig.8, but is for -20 ℃ isotherm over the southern ocean (80 ° E-90 ℃E, 50 ℃S-60 ℃S).

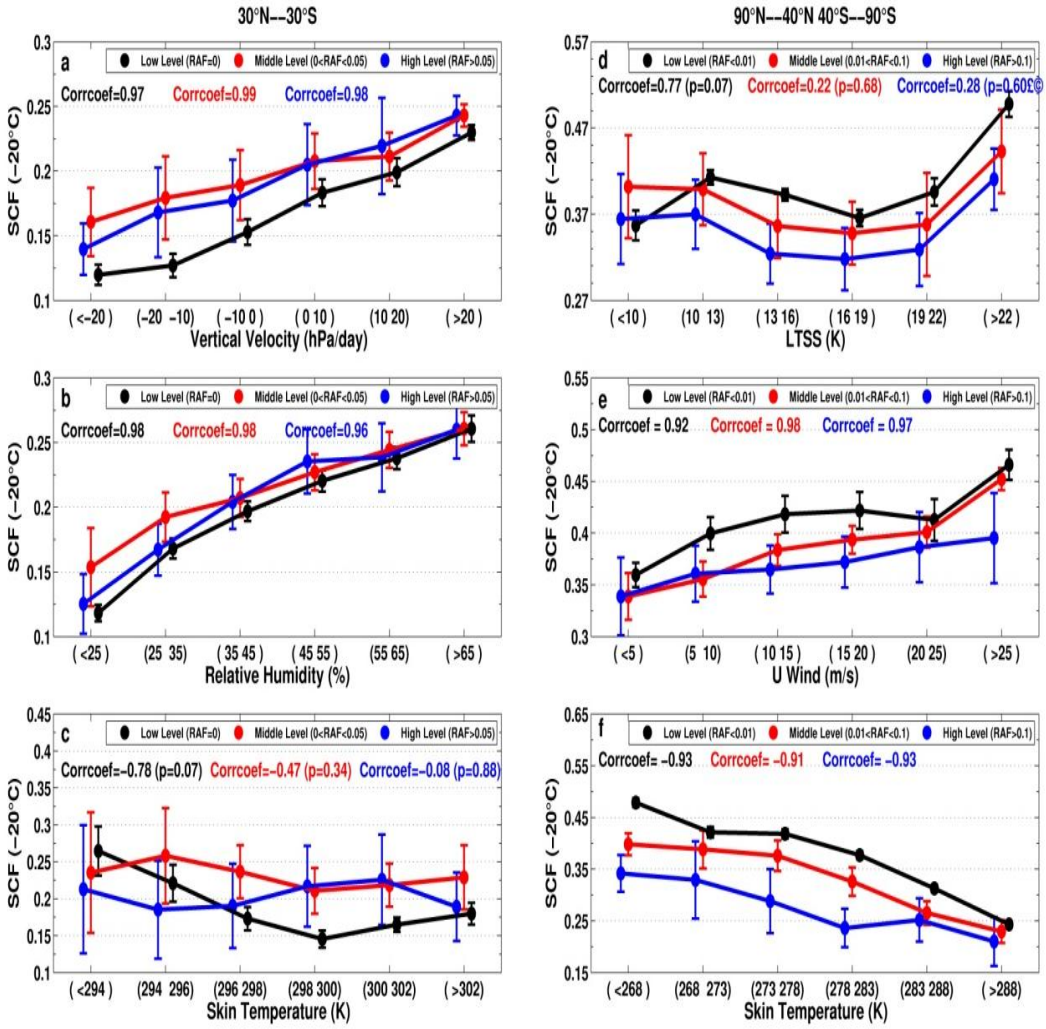

Fig.11. Spatial correlations between SCFs at -20 ℃ isotherm and meteorological parameters under different aerosol loading conditions. Left panel represents tropics, whereas right panel corresponds to the correlations in middle and high latitudes. Only those regions with temporal correlations between SCFs and meteorological parameters at the 95% confidence level are used to calculate the spatial correlations between SCFs and meteorological parameters. The confidence values (i.e., p value) are provided only when the confidence level of the spatial correlation between variables is less than 95%.